The Effect of Northern Hemisphere Winds on the Meridional Overturning Circulation and Stratification

PAOLA CESSI

Scripps Institution of Oceanography, University of California, San Diego, La Jolla, California

(Manuscript received 23 April 2018, in final form 10 August 2018)

ABSTRACT

The current paradigm for the meridional overturning cell and the associated middepth stratification is that the wind stress in the subpolar region of the Southern Ocean drives a northward Ekman flow, which, together with the global diapycnal mixing across the lower boundary of the middepth waters, feeds the upper branch of the interhemispheric overturning. The resulting mass transport proceeds to the Northern Hemisphere of the North Atlantic, where it sinks, to be eventually returned to the Southern Ocean at depth. Seemingly, the wind stress in the Atlantic basin plays no role. This asymmetry occurs because the Ekman transport in the Atlantic Ocean is assumed to return geostrophically at depths much shallower than those occupied by the interhemispheric overturning. However, this vertical separation fails in the North Atlantic subpolar gyre region. Using a conceptual model and an ocean general circulation model in an idealized geometry, we show that the westerly wind stress in the northern part of the Atlantic provides two opposing effects. Mechanically, the return of the Ekman transport in the North Atlantic opposes sinking in this region, reducing the total overturning and deepening the middepth stratification; thermodynamically, the subpolar gyre advects salt poleward, promoting Northern Hemisphere sinking. Depending on which mechanism prevails, increased westerly winds in the Northern Hemisphere can reduce or augment the overturning.

1. Introduction

A peculiar feature of the zonally and vertically integrated meridional heat transport by the ocean is its interhemispheric asymmetry: more heat is transported northward in the Northern Hemisphere than southward in the Southern Hemisphere, with a net northward transport at the equator (Trenberth and Caron 2001). This asymmetry is compensated by the atmospheric heat transport, accompanied by a shift south of the equator of the climatological position of the intertropical convergence zone (Kang et al. 2009). The oceanic heat transport in the Atlantic sector, everywhere northward, causes this asymmetry: it arises from the interhemispheric meridional overturning circulation that occupies the middepths of the Atlantic basin.

The conceptual framework for the maintenance of the middepth overturning circulation (MOC) and the associated stratification has changed in the last decades. The idea of a diffusive balance between advection of buoyancy by the global overturning and diapycnal mixing on microscales (Stommel 1958; Munk 1966; Munk and Wunsch

1998) has been replaced by a wind-driven and eddy-mediated perspective (Toggweiler and Samuels 1993; Gnanadesikan 1999; Marshall and Radko 2003; Wolfe and Cessi 2010; Marshall and Speer 2012; Nikurashin and Vallis 2012), where the Ekman transport in the subpolar region of the Southern Ocean, opposed by mesoscale eddy buoyancy fluxes, matches the MOC associated with sinking in the North Atlantic, determining the global middepth stratification and overturning. In this perspective, diapycnal diffusion plays a secondary role in the middepth overturning.

Because the MOC is a global process, it involves the circulation of the World Ocean, and in particular the MOC lower branch connects to the abyssal circulation, which is mostly expressed in the Indo-Pacific and is powered by diapycnal mixing (Lumpkin and Speer 2007; Talley 2013). The middepth cell is localized in the Atlantic basin, and we focus here on this component [i.e., the Atlantic meridional overturning circulation (AMOC)], for which diapycnal mixing is locally negligible. Several modeling studies have examined the dependence of the AMOC on the strength, shape, and position of the wind stress in the Southern Ocean (e.g., Hallberg and Gnanadesikan 2006; Sijp and England 2009;

Corresponding author: Paola Cessi, pcessi@ucsd.edu

Farneti et al. 2010; Abernathey et al. 2011), that is, in the upwelling region of the MOC, while the wind stress in the Northern Hemisphere subpolar gyre (i.e., in the sinking region of the MOC) has largely been ignored, presumably because it is considered inconsequential. One exception is the work of Klinger et al. (2003), who find that while doubling the wind stress in the Southern Ocean strengthens the MOC, doubling the wind stress in the Northern Hemisphere sinking region weakens the MOC slightly. This is perhaps surprising, because increasing wind stress anywhere should add energy to the system, resulting in a more vigorous circulation. On the other hand, increasing Ekman suction in the downwelling region of the MOC could hinder sinking and reduce the middepth overturning.

Klinger et al.'s (2003) result is in line with the data analysis of Evans et al. (2017), finding a short-term response of the AMOC between 26° and 45°N to interannual variations in the strength and position of the North Atlantic subtropical and subpolar gyres, driven by changes in the wind stress. Specifically, a decrease in the AMOC transport is associated with an increase in the amplitude of the wind stress curl. A similar correlation between the curl of the wind in the North Atlantic gyres and the salinity has been observed (Häkkinen and Rhines 2004; Hátún et al. 2005; Häkkinen et al. 2011), whereby weakening of the subpolar gyre is associated with higher salinity on interannual time scales. The effect of changes in the salinity of the subpolar gyre associated with wind changes depends on the time scale considered: changes involving the upper branch of the MOC occur on the time scale of equilibration of the upper branch of the overturning (i.e., hundreds of years). On interannual and decadal time scales, changes are associated with the dynamics of the locally wind-driven gyre.

As discussed by Jones and Cessi (2017), in the subpolar region, the gyre drives northward advection of salt in the interior (i.e., far away from the western boundary) and southward advection of freshwater in the western boundary current, resulting in a net downgradient transport of salt. The southward advection by the gyre's western boundary current competes with the northward advection associated with the MOC, also taking place along the western boundary. Thus, whether the MOC manages to advect salt northward, thus accomplishing the *salt advection feedback* that promotes deep water mass formation (Stommel 1961), depends on the relative strength of the MOC and the wind-driven subpolar gyre. If the velocity of the southward western boundary current associated with the locally wind-driven gyre exceeds the northward velocity of the western boundary current associated with the upper branch of the MOC, then the salt advection feedback mechanism is ineffective.

To have the salt advection feedback mechanism, the surface salinity must be free to evolve, and thus freshwater flux surface boundary conditions are necessary. Conversely, if surface salinity is relaxed to a prescribed distribution on a time scale shorter than the time scale of surface advection by the MOC, there is no salt advection feedback.

In this work, we systematically examine the *equilibrium* response of the MOC to changes in the Northern Hemisphere westerly wind stress. We consider a simplified model of the Atlantic sector of the World Ocean, which equilibrates in about 2000 years, ignoring the interaction with the abyssal cell, which has an even longer time scale of adjustment (many thousands of years). The approach is to consider two sets of experiments that only differ in the salinity surface boundary condition: 1) freshwater flux is prescribed at the surface, allowing the salt advection feedback to operate, and 2) salinity is rapidly relaxed to a prescribed distribution, effectively eliminating the salt advection feedback.

We find that the response to changes in the westerly winds of the Northern Hemisphere depends crucially on the presence or absence of the salt advection feedback, which is controlled by the surface boundary condition on salinity. For relaxation boundary conditions, increasing the winds deepens the stratification and weakens the cross-equatorial MOC. This behavior can be rationalized with a conceptual model in the spirit of Gnanadesikan (1999).

For freshwater flux boundary conditions, doubling or quadrupling the Northern Hemisphere westerly winds deepens the stratification and weakens the MOC. However, reducing to zero the same winds alters the circulation in a manner not predicted by the conceptual model because of a major wind-driven redistribution of the surface salinity in the subpolar region, which makes the dependence of the MOC and deep stratification nonmonotonic functions of the wind stress in the sinking region. The large changes in Northern Hemisphere stratification are transmitted by the MOC to the Southern Hemisphere, including the Antarctic Circumpolar Current, showing that just as the Southern Ocean winds can influence the circulation in the high latitudes of the North Atlantic, the Northern Hemisphere winds can alter the circulation in the Southern Ocean.

2. Conceptual model

In its simplest terms, the modern perspective on the upper branch of the AMOC is summarized by the buoyancy budget vertically integrated above a buoyancy surface within the middepth overturning, as schematically depicted in Fig. 1. It is useful to choose a buoyancy surface that approximately separates the northward-flowing upper
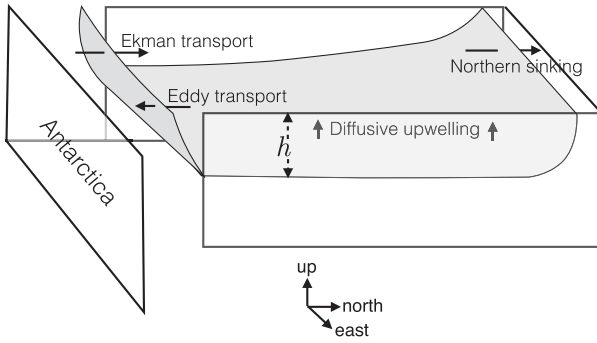
FIG. 1. Geometry of the conceptual model illustrating the budget for the residual circulation above the $\sigma_2 = 37$ kg m^{-3} surface in the middepth MOC.

branch from the southward-flowing return branch (e.g., the $\sigma_2 = 37$ kg m^{-3} surface in the top-left panel of Fig. 4). The characterizing feature of $\sigma_2 = 37$ kg m^{-3} is that it is among the densest buoyancy surfaces, which outcrops in the subpolar regions of both the Southern Ocean and the North Atlantic.

The Ekman transport in the subpolar region of the Southern Ocean is constrained to return at the ocean's bottom (or below the top of bathymetric obstacles) by the longitudinally periodic geometry of this region and thus must enter the region above the target buoyancy. Eddy buoyancy fluxes in the Southern Ocean effect some transport out of the budget region and in the process restratify the water column opposing the over-turning tendency of the northward Ekman velocity (Marshall and Radko 2003). The residual buoyancy transport proceeds northward in an interhemispheric western boundary current, augmented (diminished) in the Northern (Southern) Hemisphere by diapycnal mixing, until it sinks at the northern outcrop of the target buoyancy surface.

To close the problem, the residual overturning, eddy buoyancy fluxes, and diapycnal mixing must all be re-lated to the isopycnal slope, or the isopycnal height h. For the zonally averaged budget, Gnanadesikan (1999) proposes the following closure:[1]

$$
\underbrace{-\frac{\tau_s}{\rho f_s}}_{\text{Ekman}} - \underbrace{\kappa_{\text{GM}} \frac{h}{L_c}}_{\text{Eddy flux}} + \underbrace{\kappa_v \frac{\text{Area}}{hL_x}}_{\text{Mixing}} = \underbrace{\Delta b \frac{h^2}{f_n L_x}}_{\text{Meridional transport}}, \quad (1)
$$

where τ_s, f_s denote the zonally averaged wind stress and the Coriolis parameter at the southern boundary of the

---

[1] Several different closures for the meridional transport in the Northern Hemisphere have been proposed (Fürst and Levermann 2012): we use the one put forward by Johnson and Marshall (2002).

integration region, respectively; ρ is the reference den-sity; and L_x is the width of the Southern Ocean. The unknown in (1) is the depth of the isopycnal at the eastern boundary h, which is guaranteed to be independent of latitude until the sinking latitude is reached. The eddy flux term is parameterized as diffusion of isopycnal thickness, with eddy diffusivity κ_{GM}; the slope of the isopycnal is then approximated to be linear across the periodic Southern Ocean region of latitudinal extent L_c and depth h. Diapycnal mixing occurs over the whole area of the isopycnal with averaged diffusivity κ_v. Finally, the Eulerian meridional velocity v_n associated with the residual overturning at the northern outcrop is assumed to be in thermal wind balance and thus satisfies

$$
f_n \partial_z v_n = \partial_x b_n, \qquad (2)
$$

where b_n, f_n are the buoyancy and Coriolis parameter at the northern outcrop, respectively. The vertically and zonally integrated Eulerian meridional transport ψ_n then scales as

$$
f_n \psi_n \sim \Delta b (h^2 - h_w^2), \qquad (3)
$$

where Δb is the range of outcropped buoyancies shared between the Southern Ocean and the sinking region. Assuming that sinking occurs on the western boundary, the buoyancy depth at the western boundary h_w is much smaller than the depth at the eastern boundary h, and the scaling of the residual overturning term in (1) is obtained.

The formulation above does not include consideration of the Ekman transport (and its return flow) in the sinking region. In the subpolar gyre of the enclosed basin, the Ekman return flow occurs at depths compa-rable to those occupied by the upper branch of the MOC, and its effect can be included by adding the tur-bulent stress divergence to the longitudinal momentum balance. Instead of geostrophic balance, the Eulerian meridional velocity then obeys

$$
f_n v_n = \partial_x p_n - \partial_z \frac{\tau}{\rho}, \qquad (4)
$$

where τ is the vertical turbulent stress, satisfying the surface boundary condition $\tau = \tau_n$, with τ_n the wind stress at the sinking location and p_n the hydrostatic pressure.

It is instructive to examine the effect of the vertical turbulent stress by reviewing the dynamics of a homo-geneous buoyancy layer of depth D, floating on top of a motionless region with higher density: this is the one-and-a-half-layer version of the classical Parsons and Veronis model (Parsons 1969; Veronis 1973). In this

case, the pressure gradient is $\nabla p_n = \Delta b \nabla D$, where Δb is the buoyancy jump between the two layers, and the vertically and zonally integrated Eulerian transport ψ_n is given by

$$f_n \psi_n = \frac{\Delta b}{2} D^2 \big|_{x=\text{west}}^{x=\text{east}} - L_b \frac{\overline{\tau}_n}{\rho}, \qquad (5)$$

where the overbar indicates the zonal average, and L_b is the width of the basin in the east–west direction. If there is no MOC, $\psi_n = 0$, and D is deeper at the eastern boundary than at the western wall. The associated pressure difference is in geostrophic balance with a current that returns northward the zonally integrated southward Ekman transport. Because we are interested in the *residual* rather than the *Eulerian* overturning, it is appropriate to also add the eddy flux contribution, as is done in the Southern Ocean, but with the opposite sign for the isopycnal slopes. Thus, we define the zonally integrated residual transport $\psi^{\dagger}$ as

$$f_n \psi^{\dagger} \equiv \frac{\Delta b}{2} D^2 \big|_{x=\text{west}}^{x=\text{east}} - L_b \frac{\overline{\tau}_n}{\rho} + f_n L_b \kappa_{\text{GM}} \frac{h}{L_N}. \qquad (6)$$

The last term on the right-hand side represents the eddy flux of buoyancy in the Northern Hemisphere's subpolar gyre: it is characterized by the meridional distance L_N between the outcrop and the northern boundary, which becomes infinite when the overturning collapses.

In summary, the analysis just outlined suggests a modified scaling of the MOC buoyancy budget in (1), given by

$$\underbrace{-\frac{\tau_s}{\rho f_s}}_{\text{Ekman}} \underbrace{- \kappa_{\text{GM}} \frac{h}{L_c}}_{\text{Eddy flux}} + \underbrace{\kappa_v \frac{L_y}{h}}_{\text{Mixing}} = \underbrace{\Delta b \frac{h^2}{f_n L_x} - \frac{L_b \tau_n}{L_x \rho f_n} + \kappa_{\text{GM}} \frac{L_b h}{L_N L_x}}_{\text{Residual transport}}. \qquad (7)$$

Notice that it is the definition of the MOC transport that has changed: in the absence of Southern Ocean eddy flux or diapycnal mixing, the MOC transport would be solely determined by the Southern Ocean wind stress τ_s and would not be affected by τ_n or an eddy process in the Northern Hemisphere. There would be just a decrease in stratification (i.e., an increase in h) when τ_n is increased. However, because of Southern Ocean eddy fluxes and diapycnal mixing, the total MOC residual transport depends on h, and the increase in h due to increasing τ_n leads to a decrease in MOC sinking. The northern wind stress and eddy flux terms are multiplied by the ratio L_b/L_x, measuring the width of the sinking region relative to the width of the circumpolar region: this ratio is rather small for Atlantic sinking.

To illustrate the dependence of h and $\psi^{\dagger}$ on τ_n, it is useful to consider small perturbations of τ_n and linearize around the solution h_0, which is the solution of

$$-\frac{\tau_s}{\rho f_s} + \frac{L_b \tau_n}{L_x \rho f_s} + \kappa_v \frac{L_y}{h_0} = \Delta b \frac{h_0^2}{f_n L_x} + \kappa_{\text{GM}} \frac{h_0}{L_c} + \kappa_{\text{GM}} \frac{L_b h_0}{L_x L_N}. \qquad (8)$$

The zonally integrated residual transport $\psi_0^{\dagger}$, associated with h_0, satisfies

$$\psi_0^{\dagger} = -\frac{\tau_s}{\rho f_s} - \kappa_{\text{GM}} \frac{h_0}{L_c} + \kappa_v \frac{L_y}{h_0}. \qquad (9)$$

The leading order perturbation $h_1 \approx h - h_0$, associated with a perturbation of the northern wind stress $\delta\tau_n$, satisfies

$$h_1 \left(\frac{\kappa_{\text{GM}}}{L_c} + \kappa_v \frac{L_y}{h_0^2} + 2\Delta b \frac{h_0}{f_n L_x} + \kappa_{\text{GM}} \frac{L_b}{L_x L_N} \right) = \frac{L_b \delta\tau_n}{L_x \rho f_n}. \qquad (10)$$

Because the coefficient multiplying h_1 is positive, h_1 increases with $\delta\tau_n$, linearly for small increases. Conversely, changes in the zonally integrated residual transport *decrease* with increasing northern westerlies according to

$$\psi_1^{\dagger} = -h_1 \left(\frac{\kappa_{\text{GM}}}{L_c} + \kappa_v \frac{L_y}{h_0^2} \right). \qquad (11)$$

3. Results of a general circulation model

The effect of τ_n on the MOC and stratification predicted by the scaling in (7) is tested in an ocean general circulation model (GCM), configured in an idealized Atlantic sector of the global ocean. The model is the MITgcm (Marshall et al. 1997), which numerically solves the primitive equations in a spherical sector 60° wide with solid boundaries to the north and south at $\pm 70°$. The solid boundaries along the meridians at 0° and 60°, terminate south of $-52°$, where the domain becomes periodic in longitude. This 60°-periodic region represents the circumpolar portion of the Southern Ocean in the Atlantic sector, so in the notation of (7), $L_b = L_x$. The domain is 4000 m deep, except that south of the eastern boundary, there is a 1°-wide ridge 2000 m high. The model's resolution is 1° in latitude and longitude. In the vertical direction, there are 50 unequally spaced levels, with depths ranging from 17 m near the surface to 148 m at the bottom. The nonlinear equation of state by Jackett and McDougall (1995) is used. Because the resolution is insufficient to permit the development of
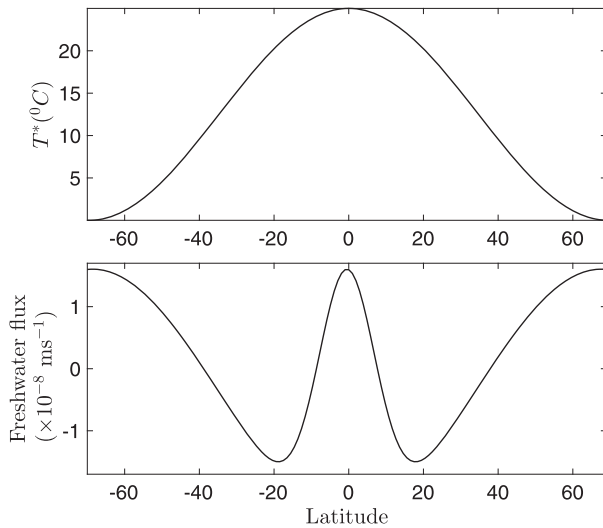
FIG. 2. (top) Relaxation temperature to which the model surface temperature is relaxed on a time scale of 15 days. (bottom) Surface freshwater flux. The salinity (virtual) flux imposed at the model's surface is the negative of the freshwater flux, multiplied by the reference salinity (35 psu).
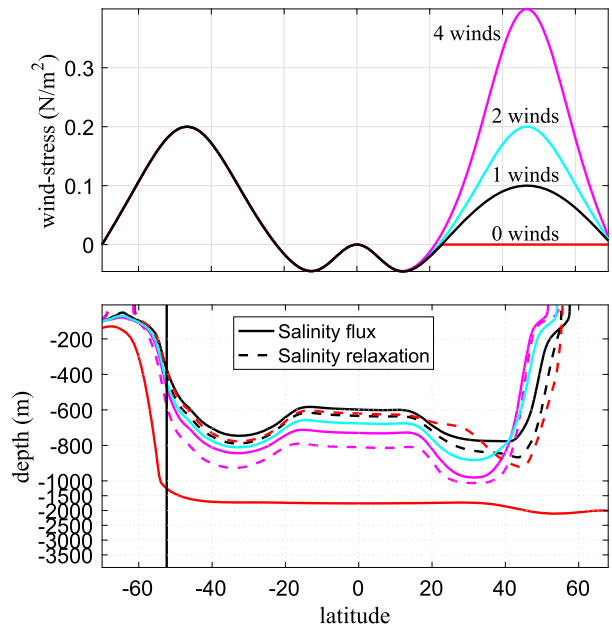

FIG. 3. (top) The wind stress profiles used in the computations as a function of latitude, labeled with the names used in subsequent figures. (bottom) Contours of the zonally averaged potential density surfaces $\sigma_2 = 37 \, \mathrm{kg \, m}^{-3}$ in the latitude–depth plane for the different wind stress profiles, with colors matching the wind profiles of the top panel. Solid lines are for the experiments with fixed flux salinity boundary condition, and dashed lines are for the relaxation boundary condition.

baroclinic eddies, their effect on tracer transport is parameterized using the Gent–McWilliams advective form (Gent and McWilliams 1990; Griffies 1998; Ferrari et al. 2010) and the isopycnal tracer mixing described by Redi (1982), with equal constant coefficients of eddy diffusivity $\kappa_{\mathrm{GM}} = \kappa_{\mathrm{Redi}} = 500 \, \mathrm{m}^2 \, \mathrm{s}^{-1}$. The vertical diffusivity is set to $2 \times 10^{-5} \, \mathrm{m}^2 \, \mathrm{s}^{-1}$ in the interior, increasing to $1 \times 10^{-2} \, \mathrm{m}^2 \, \mathrm{s}^{-1}$ at the surface over a depth of 30 m to model the mixed layer. A simple convective adjustment scheme is used where vertical tracer diffusivity is increased to $10 \, \mathrm{m}^2 \, \mathrm{s}^{-1}$ when stratification is statically unstable.

The surface forcing is prescribed as steady zonally uniform wind stress (shown in the top panel of Fig. 3) and relaxation to temperature with a time scale of 15 days (shown in the top panel of Fig. 2). Two sets of experiments are performed, differing in the surface salinity boundary condition: in the first set of experiments, a zonally uniform freshwater flux (virtual salt flux) is prescribed (shown in the bottom panel of Fig. 2); in the second set of experiments, the sea surface salinity (SSS) is relaxed on a time scale of 30 days to the time-averaged, two-dimensional distribution of SSS obtained for the fixed flux experiment with the ''control'' wind stress value (the black line profile in the top panel of Fig. 3). In each set of experiments, the surface wind stress is varied, while the temperature and salinity forcings are kept fixed, as just described.

Figure 3 (bottom panel) shows the time- and zonally averaged depths of the $\sigma_2 = 37 \, \mathrm{kg \, m}^{-3}$ potential density surfaces, color coded for the four different profiles of the

surface wind stress (shown in the top panel) for both the fixed flux (solid lines) and relaxation surface salinity boundary conditions (dashed lines). The $\sigma_2 = 37 \, \mathrm{kg \, m}^{-3}$ depth, which is representative of the middepth region of the MOC, is displaced downward in most of the domain as the wind stress in the sinking region is increased, as predicted by the conceptual model in (7), and more so for the relaxation boundary condition. However, for the fixed flux boundary condition, when the Northern Hemisphere westerly wind stress is decreased to zero (red solid line), the $\sigma_2 = 37 \, \mathrm{kg \, m}^{-3}$ surface is deepened so much that it no longer outcrops in the Northern Hemisphere, indicating that the overturning is confined to shallower levels.

In the following, we discuss in more detail the role of the Northern Hemisphere wind stress on the stratification and overturning, beginning with the fixed freshwater flux boundary condition, even though the salt advection complicates the dynamics in this case. The dynamics of the salinity relaxation boundary condition case are simpler and are largely described by the conceptual model of section 2. However, because the distribution of surface salinity used in the relaxation boundary condition case is derived from the fixed flux control experiment, this set of computations is discussed first.
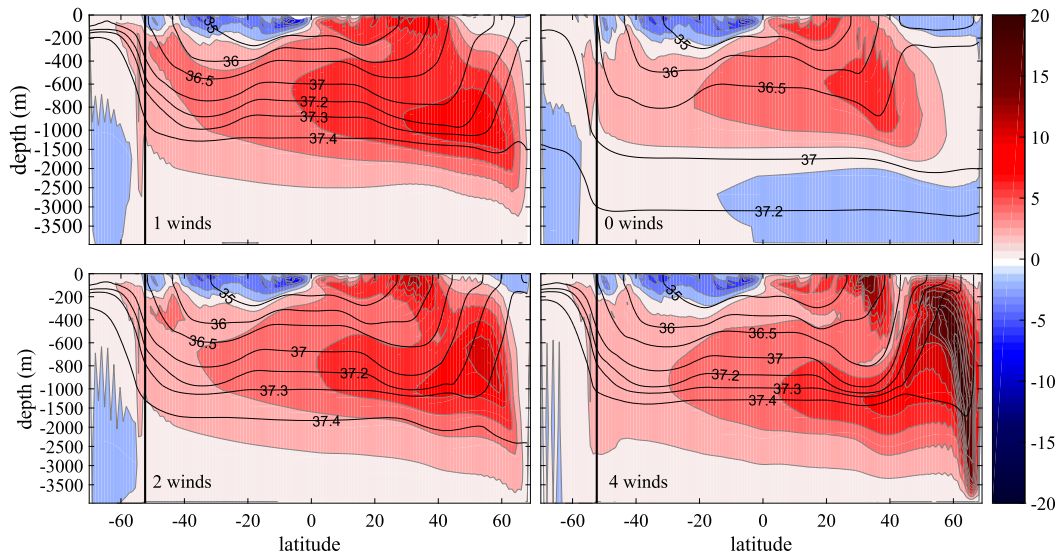
FIG. 4. Thickness-weighted residual overturning streamfunction (Sv) obtained by integrating the Eulerian plus the Gent–McWilliams bolus meridional velocity from the bottom to different σ_2 levels, then time averaged and zonally integrated (colors and gray contours; contour interval is 2 Sv), as a function of latitude and σ_2, for four computations forced by the different wind stress profiles given in the top panel of Fig. 3 with freshwater flux surface boundary conditions. The ordinate is remapped in depth coordinates using the accumulated σ_2 thickness. Selected zonally averaged σ_2 isocontours (kg m^{-3}) are shown in black contours.

a. Fixed freshwater flux surface boundary condition

A nonmonotonic dependence on the Northern Hemisphere wind stress amplitude is also found for the meridional overturning circulation, measured here by the thickness-weighted residual meridional streamfunction, obtained by integrating the meridional velocity (Eulerian plus Gent–McWilliams bolus component) from the bottom to a specified set of fifty σ_2 levels, then time averaging and zonally integrating it (Young 2012). In this way, the meridional buoyancy transport due to the Eulerian velocity, gyres, stationary waves, and parameterized eddies is captured. Figure 4 shows the resulting overturning streamfunction for the four wind stress profiles shown in the top panel of Fig. 3. With the westerly wind stress in the Northern Hemisphere doubled (Fig. 4, bottom-left panel), the overturning is decreased relative to the control wind everywhere, except in a region under the wind stress maximum. In particular, the cross-equatorial transport of the interhemispheric cell is reduced (see Fig. 6, orange dashed lines and circles, right axis), although the maximum streamfunction (at the latitude of the westerlies) is increased.

With the westerly wind stress quadrupled (Fig. 4, bottom-right panel), the overturning circulation above 1000 m is reduced again, except at the latitudes of the wind stress maximum. However, below 1000 m, the circulation is stronger for the quadrupled wind stress, and the circulation is strongly intensified near the northern

boundary. The northern intensification is associated with a locally enhanced pycnostad, where the parameterized eddy flux (inversely proportional to the local stratification) is very large (see Fig. 5, bottom-right panel). Because the parameterized eddy flux acts to transport buoyancy poleward, it produces an overturning that in the Northern Hemisphere is in the same sense as the MOC, and thus reinforces it. This is in contrast with the effect of the eddy flux in the Southern Hemisphere, where the poleward eddy flux contrasts the interhemispherical overturning.

Finally, for the zeroed westerly wind stress, the overturning circulation is weakened everywhere (top-right panel in Fig. 4): in this case, there are essentially no isopycnals shared between the circumpolar region and the Northern Hemisphere, so the overturning is confined to shallower levels. In particular, the isopycnals denser than $\sigma_2 = 36.5$ kg m^{-3} no longer outcrop in the Northern Hemisphere.

The change in stratification due to the wind stress in the Northern Hemisphere also causes changes in the zonal transport of the circumpolar current, as can be seen in the barotropic streamfunction associated with the vertically integrated velocity, shown in Fig. 7. The small deepening of the middepth isopycnals as the northern wind stress increases, and the associated slope increase in the circumpolar region, induces a small increase in the transport of the zonal circumpolar current
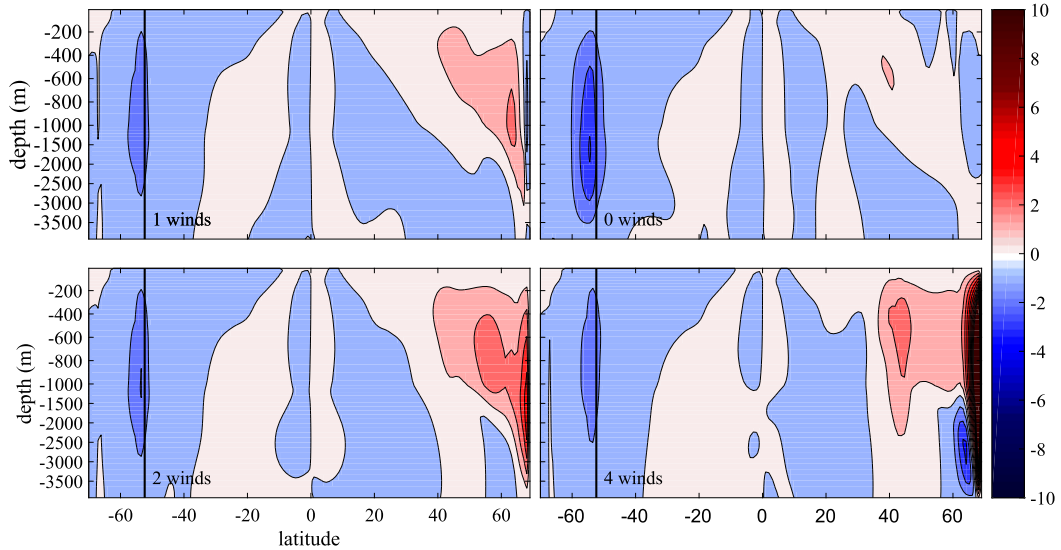
FIG. 5. Overturning streamfunction (Sv) associated with the time-averaged and zonal integral of the Gent–McWilliams bolus velocity (contour interval is 2 Sv), as a function of latitude and depth, for four computations forced by the different wind stress profiles given in the top panel of Fig. 3.

(Fig. 6, blue solid curve and asterisks, left axis). When the westerly wind stress goes to zero, the substantial weakening of the overturning leads to a sizable steepening of the middepth isopycnals. The steepening of the isopycnal slope in the circumpolar region can be deduced by (7), rearranged to yield

$$-\kappa_{GM}\frac{h}{L_c} = \frac{\tau_s}{\rho f_s} - \kappa_v \frac{L_y}{h} + \frac{\psi^\dagger}{L_x}, \qquad (12)$$

where $\psi^\dagger$ is defined in (6). The first two terms on the right-hand side are negative ($f_s < 0$ is the Coriolis parameter in the circumpolar region), but the middepth overturning $\psi^\dagger$ is positive and thus tends to reduce the (negative) isopycnal slope. When $\tau_n = 0$, the meridional overturning retreats north of the circumpolar region, so that the circumpolar stratification is in the zero residual transport limit considered by Marshall and Radko (2003). The associated increase in h/L_c leads, through thermal wind balance, to strengthening of the zonal circumpolar transport. This remote effect of wind stress in the Northern Hemisphere changing the circumpolar transport, mediated by a global rearrangement of the middepth stratification and overturning circulation, would probably be reduced in a more realistic setting with a narrower longitudinal width in the sinking region relative to the circumpolar width.

In addition, it is not clear whether the increase in the zonal circumpolar transport would be as large with a more faithful representation of the eddy flux of tracers: the literature on eddy saturation indicates that an increase

in the *local* wind stress leads to a small increase in the zonal circumpolar transport (Straub 1993; Hallberg and Gnanadesikan 2001; Hogg et al. 2008; Farneti et al. 2010; Munday et al. 2013), because eddy transport of
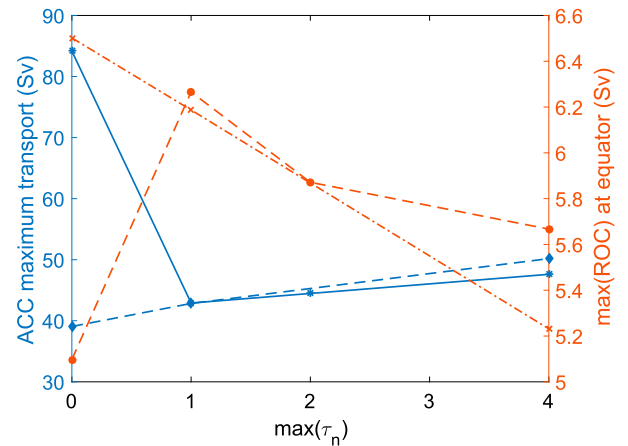

FIG. 6. Vertically and meridionally integrated zonal transport across the periodic portion of the domain (latitudes between 70° and 52.5°S) as a function of the maximum westerly wind stress amplitude in the Northern Hemisphere (blue lines; left axis): the blue solid line and asterisks are for the fixed flux boundary condition, and the blue dashed line and diamonds are for the relaxation boundary condition. Maximum residual transport across the equator as a function of the maximum westerly wind stress amplitude in the Northern Hemisphere (orange lines; right axis): the orange dashed line and circles are for the fixed flux boundary condition, and the orange dashed–dotted line and × marks are for the relaxation boundary condition.

momentum (due to both barotropic and baroclinic eddies) also increases counteracting the overturning associated with the increased Ekman transport. The effect of remote wind stress on the circumpolar transport has not been studied in the eddy-resolving context, but presumably some eddy-saturation effects would still be operative.

In summary, the computations partially confirm the prediction of the conceptual model of section 2 and the scaling in (7): the middepth isopycnals deepen as the northern wind stress is increased, and the interhemispheric transport decreases. However, more complex behavior is also obtained that is not predicted by (7): for zero northern wind stress, fewer isopycnals are shared with the circumpolar region, and the circulation is greatly reduced.

This nonmonotonic behavior can be rationalized by looking at the changes in the salinity induced by the wind-driven perturbations. Specifically, we focus on the salinity at the surface, which is representative of the whole upper branch of the MOC. Figure 8 shows the sea surface salinity (color contours and thin black lines) for the four wind stress profiles shown in the upper panel of Fig. 3: the main differences are found in the Northern Hemisphere subpolar gyre region. As the local wind stress increases, high salinity values from the subtropical region are advected northward by the cyclonic wind-driven circulation, increasing the salinity in the subpolar gyre, especially on the eastern side. In particular, while for the control wind profile the lowest salinities in the Northern and Southern Hemispheres' subpolar regions are comparable ("1 winds" panel in Fig. 8), as the wind increases the subpolar Northern Hemisphere salinity becomes larger than its Southern Hemisphere counterpart ("2 winds" and "4 winds" panels in Fig. 8), creating the conditions for the establishment of the thick pycnostad, which in turn leads to the clockwise circulation associated with the eddy flux parameterization. Conversely, when the northern wind stress is zeroed, the subpolar gyre becomes extremely fresh, reducing the range of outcropping isopycnals shared with the circumpolar region ("0 winds" panel in Fig. 8) and the strength of the overturning. Figure 8 (thick red line) also shows the outcrop of the time-averaged $\sigma_2 = 37\,\mathrm{kg\,m}^{-3}$: as the wind stress increases, the outcrop area increases in the Northern Hemisphere and decreases in the circumpolar region. For zeroed wind stress, the time-averaged $\sigma_2 = 37\,\mathrm{kg\,m}^{-3}$ surface no longer outcrops, leading to a near collapse of the middepth overturning.

In these computations, the salinity in the subpolar gyre is determined by a competition between two opposing effects. On one hand, as the Northern Hemisphere westerly wind stress increases, there is deepening of the isopycnals and a decreased residual overturning, as predicted by (7). This leads to a decreased northward salinity advection by the northward western boundary current associated with the overturning (the salt advection feedback) (Stommel 1961; Rahmstorf 1996). On the other hand, the increased wind stress spins up the Northern Hemisphere subpolar/subtropical gyres (cf. Fig. 7), leading to a decreased salinity jump across the intergyre boundary, as predicted by the scaling of Jones and Cessi (2017, their appendix B), resulting in a more saline subpolar gyre. In the configuration examined here, where the circumpolar region has a small longitudinal extent, the interhemispheric MOC is weak (about 6 Sv; $1\,\mathrm{Sv} \equiv 10^6\,\mathrm{m}^3\,\mathrm{s}^{-1}$), and the Northern Hemisphere locally wind-driven flows dominate over the salinity advection by the MOC for all values of the Northern Hemisphere wind stress except zero.

b. Relaxation surface boundary condition

The salinity feedback is essential for the dramatic changes seen for zero wind stress in the northern subpolar gyre. In the following, the salinity feedback is removed by replacing the freshwater flux surface boundary condition with relaxation to a prescribed surface salinity distribution. Specifically, the surface salinity is relaxed to the time-averaged SSS obtained when the Northern Hemisphere wind stress is set to the control value (i.e., the black line profile in the top panel of Fig. 3: "1 wind"): this is the SSS shown in the leftmost panel of Fig. 8. The 30-day relaxation time is much shorter than the advection time around the subpolar gyre, which is on the order of 20 years for the control experiment.

Figure 3 (bottom panel, dashed lines) shows that the isopycnal depth increases monotonically with the Northern Hemisphere wind for the relaxation boundary condition. This leads to a qualitative change in the response to the zero wind stress profile relative to the freshwater flux experiments in that the depth of the isopycnal increases monotonically with increasing wind. The isopycnal depth increase is accompanied by a reduction in the residual overturning circulation, as measured by the cross-equatorial transport (see Fig. 9 and the dashed–dotted orange line and crosses in Fig. 6). The overall stratification is also decreased with relaxation boundary conditions: the isopycnal $\sigma_2 = 37.4\,\mathrm{kg\,m}^{-3}$ does not exist with this boundary condition for any of the wind stress configurations. Evidently, this buoyancy value exists at the surface in the time-dependent SSS, but not in the time-average used in the relaxation boundary condition.

The behavior found for the salinity relaxation surface boundary condition is in agreement with the findings of Klinger et al. (2003), who used the same type of boundary
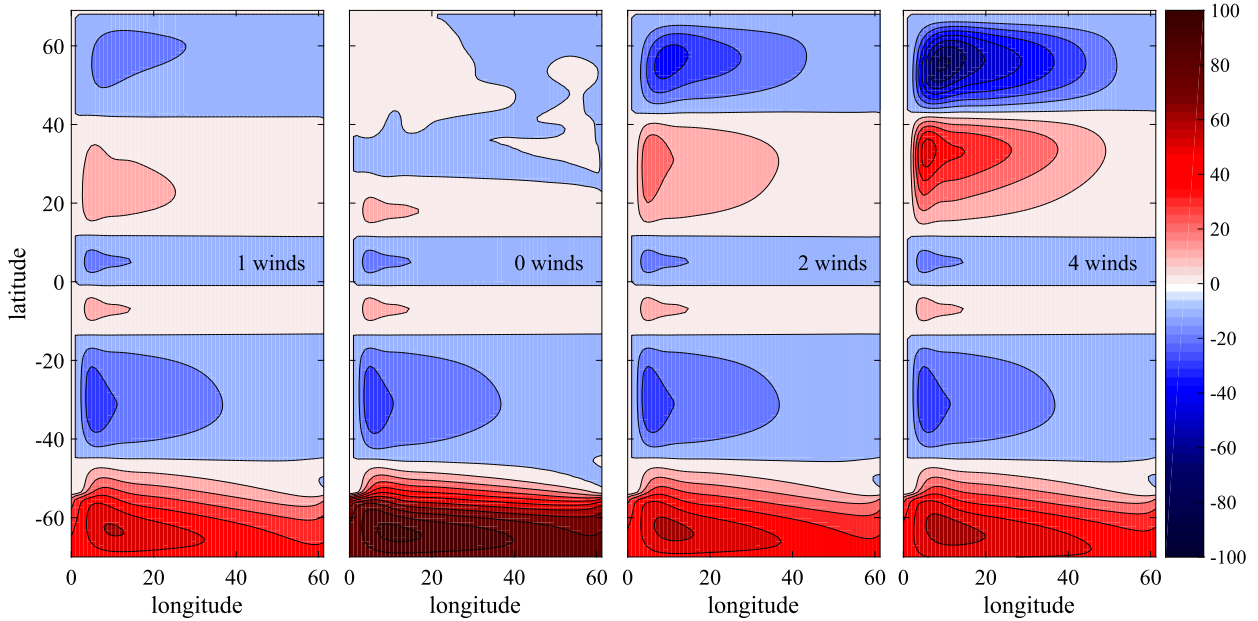
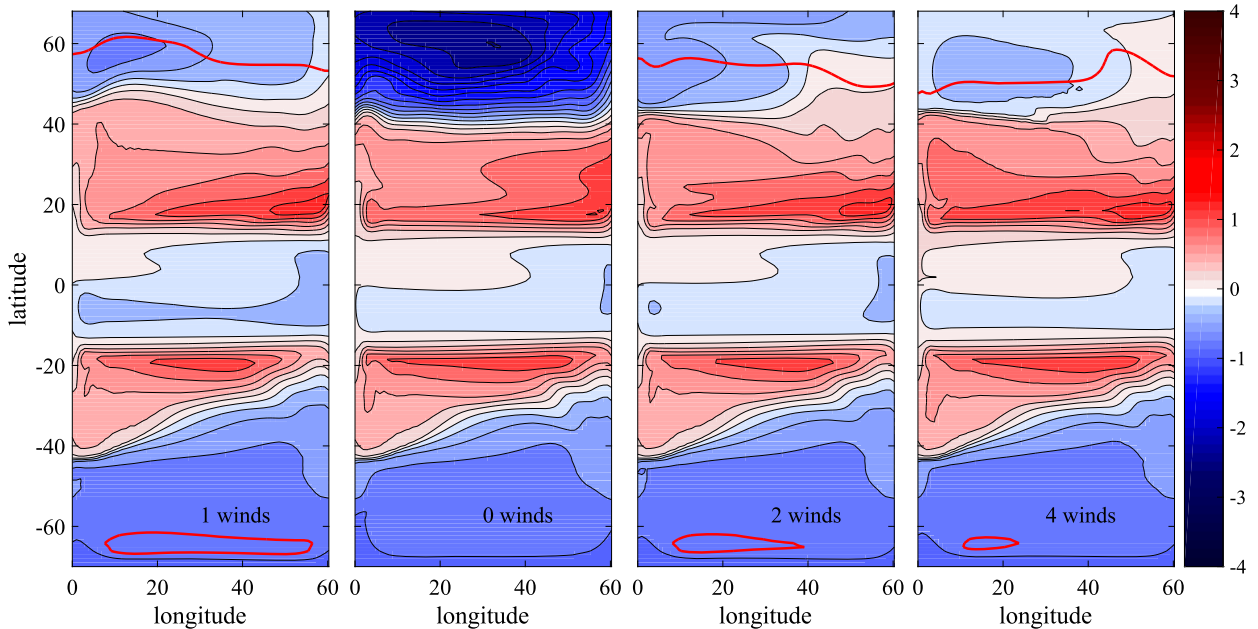FIG. 7. Barotropic streamfunction (Sv) associated with the vertically integrated velocity for four computations forced by the different wind stress profiles given in the top panel of Fig. 3 and freshwater flux surface boundary condition. The contour interval is 10 Sv.

condition. With the salinity advection feedback excluded, the conceptual model of section 2 qualitatively captures the dependence of the stratification and overturning as τ_n is changed. To account for the changes observed in the fixed salinity flux boundary condition, a more complete model would have to take into consideration the effect of the salinity feedbacks on the parameters Δb and L_n of (1), as in the approach of Johnson et al. (2007).

FIG. 8. SSS referenced to 35 psu for four computations forced by the different wind stress profiles given in the top panel of Fig. 3 and freshwater flux surface boundary condition. The contour interval is 0.2 psu. The thick red contour shows the position at the sea surface of the time-averaged $\sigma_2 = 37 \text{ kg m}^{-3}$ (i.e., its time-averaged outcrop).
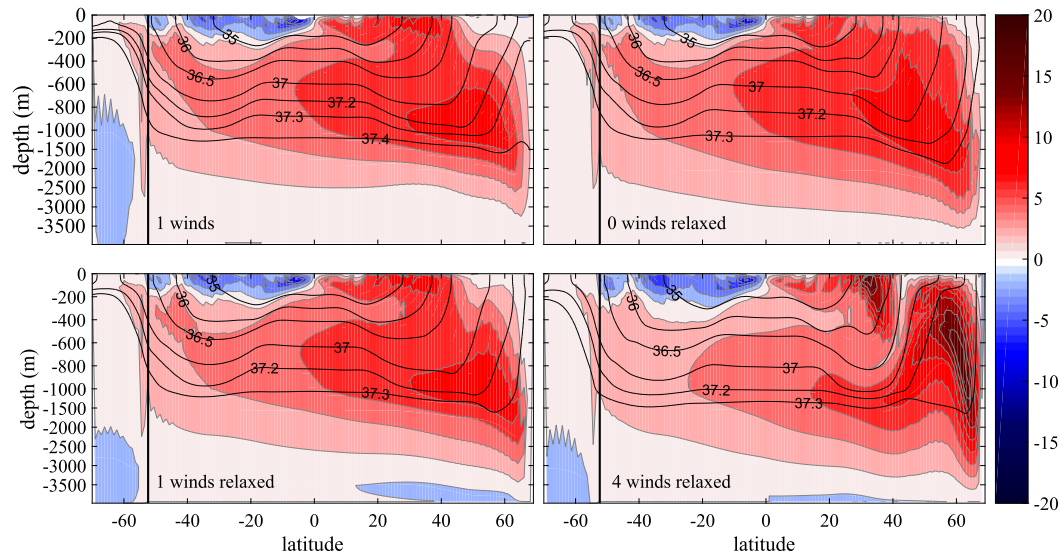
FIG. 9. Thickness-weighted residual overturning streamfunction (Sv) obtained by integrating the Eulerian plus the Gent–McWilliams bolus meridional velocity from the bottom to different σ_2 levels, then time averaged and zonally integrated (colors and gray contours; contour interval is 2 Sv), as a function of latitude and σ_2, for three computations forced by the different wind stress profiles given in the top panel of Fig. 3 with surface salinity relaxation boundary conditions. The top-left panel shows the control experiment with freshwater flux surface boundary condition. The ordinate is remapped in depth coordinates using the accumulated σ_2 thickness. Selected zonally averaged σ_2 isocontours (kg m^{-3}) are shown in black contours.

4. Discussion

The westerly wind stress in the Northern Hemisphere affects the middepth overturning circulation and stratification beyond the locally forced region. Generally, a wind stress increase tends to deepen the stratification, just as an increase in the wind stress in the Southern Ocean does, but it decreases the interhemispheric transport by the middepth overturning circulation (i.e., the opposite to the response to circumpolar winds). The mechanical response to the changes in the wind stress in the northern subpolar gyre is captured by a simple modification of Gnanadesikan's (1999) model (i.e., adding the local Ekman and eddy flux transports in the sinking region).

When the surface salinity is free to evolve, under freshwater flux boundary conditions, this remote response is not monotonic, and for zero (and presumably also for weakened) Northern Hemisphere westerly wind stress, the overturning is much reduced and the stratification is deepened. Conversely, an increase in the wind stress in the Southern Ocean leads to a monotonic increase in the middepth overturning circulation and a deepening of the stratification (Hallberg and Gnanadesikan 2006; Sijp and England 2009; Farneti and Delworth 2010; Abernathey et al. 2011).

This qualitative difference, arising from the different geometries of the two subpolar regions, is due to the

poleward salt advection effected by the wind-driven gyre, a process that is absent in the circumpolar setting. For zero winds, the salt advection by the northern subpolar gyre is absent, and the SSS becomes very fresh because of the freshwater flux applied at the surface, which is balanced just by small lateral eddy diffusion in the mixed layer, a process that is rather inefficient at exchanging salt across the boundary between the subpolar and subtropical gyres. In addition, the subpolar gyre Ekman suction pulls dense isopycnals toward the surface, increasing the range of surface buoyancy values shared with the circumpolar region, which is an essential ingredient for the quasi-adiabatic dynamics of the middepth cell (Wolfe and Cessi 2010; Nikurashin and Vallis 2012).

The salinity response to changes in the Northern Hemisphere wind stress found here is opposite to that described by Häkkinen et al. (2011): here, salinity in the subpolar gyre increases as the gyres spin up and the outcropped region expands, especially on the eastern side of the domain (cf. the leftmost three panels of Figs. 7 and 8), while in Häkkinen et al. (2011), salinity increases as the gyres spin down. There are at least two reasons for this discrepancy. First, the equilibrium response was considered here, while the observations cited above deal with interannual response, and the two cannot be compared directly. Second, in the computations

presented here, the interhemispheric overturning is weak, about 6 Sv, due to the reduced longitudinal extent of the circumpolar region, and this value is much less than the wind-driven transport in the subpolar gyre for all values of the wind stress (except zero). The observed interhemispheric AMOC transport is about 17 Sv at 26.5°N (McCarthy et al. 2015), which is comparable to the 20-Sv transport of the subpolar gyre (Colin de Verdière and Ollitrault 2016).

In nature, the wind stress acts all along the circumpolar region (i.e., along a wider stretch of longitudes at the upwelling end of the global overturning circulation than at the downwelling end). In the limited domain considered here, this disparity is not taken into account, and the global effects of the westerly wind stress in the sinking region are likely exaggerated relative to the winds in the circumpolar ocean. Nevertheless, it is clear that the wind gyres in the Northern Hemisphere have an important role in the salinity budget of the subpolar region, with implications for the global overturning circulation.

REFERENCES

Abernathey, R., J. Marshall, and D. Ferreira, 2011: The dependence of Southern Ocean meridional overturning on wind stress. *J. Phys. Oceanogr.*, **41**, 2261–2278, https://doi.org/10.1175/JPO-D-11-023.1.

Colin de Verdière, A., and M. Ollitrault, 2016: A direct determination of the World Ocean barotropic circulation. *J. Phys. Oceanogr.*, **46**, 255–273, https://doi.org/10.1175/JPO-D-15-0046.1.

Evans, D. G., J. Toole, G. Forget, J. D. Zika, A. C. N. Garabato, A. J. G. Nurser, and L. Yu, 2017: Recent wind-driven variability in Atlantic water mass distribution and meridional overturning circulation. *J. Phys. Oceanogr.*, **47**, 633–647, https://doi.org/10.1175/JPO-D-16-0089.1.

Farneti, R., and T. L. Delworth, 2010: The role of mesoscale eddies in the remote oceanic response to altered Southern Hemisphere winds. *J. Phys. Oceanogr.*, **40**, 2348–2354, https://doi.org/10.1175/2010JPO4480.1.

——, ——, A. J. Rosati, S. M. Griffies, and F. Zeng, 2010: The role of mesoscale eddies in the rectification of the Southern Ocean response to climate change. *J. Phys. Oceanogr.*, **40**, 1539–1557, https://doi.org/10.1175/2010JPO4353.1.

Ferrari, R., S. M. Griffies, A. J. G. Nurser, and G. K. Vallis, 2010: A boundary-value problem for the parameterized mesoscale eddy transport. *Ocean Modell.*, **32**, 143–156, https://doi.org/10.1016/j.ocemod.2010.01.004.

Fürst, J. J., and A. Levermann, 2012: A minimal model for wind- and mixing-driven overturning: Threshold behavior for both driving mechanisms. *Climate Dyn.*, **38**, 239–260, https://doi.org/10.1007/s00382-011-1003-7.

Gent, P., and J. C. McWilliams, 1990: Isopycnal mixing in ocean circulation models. *J. Phys. Oceanogr.*, **20**, 150–155, https://doi.org/10.1175/1520-0485(1990)020<0150:IMIOCM>2.0.CO;2.

Gnanadesikan, A., 1999: A simple predictive model for the structure of the oceanic pycnocline. *Science*, **283**, 2077–2079, https://doi.org/10.1126/science.283.5410.2077.

Griffies, S. M., 1998: The Gent–McWilliams skew flux. *J. Phys. Oceanogr.*, **28**, 831–841, https://doi.org/10.1175/1520-0485(1998)028<0831:TGMSF>2.0.CO;2.

Häkkinen, S., and P. B. Rhines, 2004: Decline of subpolar North Atlantic circulation during the 1990s. *Science*, **304**, 555–559, https://doi.org/10.1126/science.1094917.

——, ——, and D. L. Worthen, 2011: Warm and saline events embedded in the meridional circulation of the northern North Atlantic. *J. Geophys. Res.*, **116**, C03006, https://doi.org/10.1029/2010JC006275.

Hallberg, R., and A. Gnanadesikan, 2001: An exploration of the role of transient eddies in determining the transport of a zonally reentrant current. *J. Phys. Oceanogr.*, **31**, 3312–3330, https://doi.org/10.1175/1520-0485(2001)031<3312:AEOTRO>2.0.CO;2.

——, and ——, 2006: The role of eddies in determining the structure and response of the wind-driven Southern Hemisphere overturning: Results from the Modeling Eddies in the Southern Ocean (MESO) project. *J. Phys. Oceanogr.*, **36**, 2232–2252, https://doi.org/10.1175/JPO2980.1.

Hátún, H., A. B. Sandø, H. Drange, B. Hansen, and H. Valdimarsson, 2005: Influence of the Atlantic subpolar gyre on the thermohaline circulation. *Science*, **309**, 1841–1844, https://doi.org/10.1126/science.1114777.

Hogg, A., M. P. Meredith, J. R. Blundell, and C. Wilson, 2008: Eddy heat fluxes in the Southern Ocean: Response to variable wind forcing. *J. Climate*, **21**, 608–620, https://doi.org/10.1175/2007JCLI1925.1.

Jackett, D. R., and T. J. McDougall, 1995: Minimal adjustment of hydrographic profiles to achieve static stability. *J. Atmos. Oceanic Technol.*, **12**, 381–389, https://doi.org/10.1175/1520-0426(1995)012<0381:MAOHPT>2.0.CO;2.

Johnson, H. L., and D. P. Marshall, 2002: A theory for the surface Atlantic response to thermohaline variability. *J. Phys. Oceanogr.*, **32**, 1121–1132, https://doi.org/10.1175/1520-0485(2002)032<1121:ATFTSA>2.0.CO;2.

——, ——, and D. A. J. Sproson, 2007: Reconciling theories of a mechanically driven meridional overturning circulation with thermohaline forcing and multiple equilibria. *Climate Dyn.*, **29**, 821–836, https://doi.org/10.1007/s00382-007-0262-9.

Jones, C. S., and P. Cessi, 2017: Size matters: Another reason why the Atlantic is saltier than the Pacific. *J. Phys. Oceanogr.*, **47**, 2843–2859, https://doi.org/10.1175/JPO-D-17-0075.1.

Kang, S. M., D. M. W. Frierson, and I. M. Held, 2009: The tropical response to extratropical thermal forcing in an idealized

GCM: The importance of radiative feedbacks and convective parameterization. *J. Atmos. Sci.*, **66**, 2812–2827, https://doi.org/10.1175/2009JAS2924.1.

Klinger, B., S. Drijfhout, J. Marotzke, and J. R. Scott, 2003: Sensitivity of basinwide meridional overturning to diapycnal diffusion and remote wind forcing in an idealized Atlantic–Southern Ocean geometry. *J. Phys. Oceanogr.*, **33**, 249–266, https://doi.org/10.1175/1520-0485(2003)033<0249:SOBMOT>2.0.CO;2.

Lumpkin, R., and K. Speer, 2007: Global ocean meridional overturning. *J. Phys. Oceanogr.*, **37**, 2550–2562, https://doi.org/10.1175/JPO3130.1.

Marshall, J., and T. Radko, 2003: Residual-mean solutions for the Antarctic Circumpolar Current and its associated overturning circulation. *J. Phys. Oceanogr.*, **33**, 2341–2354, https://doi.org/10.1175/1520-0485(2003)033<2341:RSFTAC>2.0.CO;2.

——, and K. Speer, 2012: Closure of the meridional overturning circulation through Southern Ocean upwelling. *Nat. Geosci.*, **5**, 171–180, https://doi.org/10.1038/ngeo1391.

——, C. Hill, L. Perelman, and A. Adcroft, 1997: Hydrostatic, quasi-hydrostatic, and nonhydrostatic ocean modeling. *J. Geophys. Res.*, **102**, 5733–5752, https://doi.org/10.1029/96JC02776.

McCarthy, G., and Coauthors, 2015: Measuring the Atlantic meridional overturning circulation at 26°N. *Prog. Oceanogr.*, **130**, 91–111, https://doi.org/10.1016/j.pocean.2014.10.006.

Munday, D. R., H. L. Johnson, and D. P. Marshall, 2013: Eddy saturation of equilibrated circumpolar currents. *J. Phys. Oceanogr.*, **43**, 507–532, https://doi.org/10.1175/JPO-D-12-095.1.

Munk, W. H., 1966: Abyssal recipes. *Deep-Sea Res. Oceanogr. Abstr.*, **13**, 707–730, https://doi.org/10.1016/0011-7471(66)90602-4.

——, and C. Wunsch, 1998: Abyssal recipes II: Energetics of tidal and wind mixing. *Deep-Sea Res. I*, **45**, 1977–2010, https://doi.org/10.1016/S0967-0637(98)00070-3.

Nikurashin, M., and G. Vallis, 2012: A theory of the interhemispheric meridional overturning circulation and associated stratification. *J. Phys. Oceanogr.*, **42**, 1652–1667, https://doi.org/10.1175/JPO-D-11-0189.1.

Parsons, A. T., 1969: A two-layer model of Gulf Stream separation. *J. Fluid Mech.*, **39**, 511–528, https://doi.org/10.1017/S0022112069002308.

Rahmstorf, S., 1996: On the freshwater forcing and transport of the Atlantic thermohaline circulation. *Climate Dyn.*, **12**, 799–811, https://doi.org/10.1007/s003820050144.

Redi, M. H., 1982: Oceanic isopycnal mixing by coordinate rotation. *J. Phys. Oceanogr.*, **12**, 1154–1158, https://doi.org/10.1175/1520-0485(1982)012<1154:OIMBCR>2.0.CO;2.

Sijp, W. P., and M. H. England, 2009: Southern Hemisphere westerly wind control over the ocean's thermohaline circulation. *J. Climate*, **22**, 1277–1286, https://doi.org/10.1175/2008JCLI2310.1.

Stommel, H., 1958: The abyssal circulation. *Deep-Sea Res.*, **5**, 80–82, https://doi.org/10.1016/S0146-6291(58)80014-4.

——, 1961: Thermohaline convection with two stable regimes of flow. *Tellus*, **13**, 224–230, https://doi.org/10.3402/tellusa.v13i2.9491.

Straub, D. N., 1993: On the transport and angular momentum balance of channel models of the Antarctic Circumpolar Current. *J. Phys. Oceanogr.*, **23**, 776–782, https://doi.org/10.1175/1520-0485(1993)023<0776:OTTAAM>2.0.CO;2.

Talley, L. D., 2013: Closure of the global overturning circulation through the Indian, Pacific, and Southern Oceans: Schematics and transports. *Oceanography*, **26** (1), 80–97, https://doi.org/10.5670/oceanog.2013.07.

Toggweiler, J. R., and B. Samuels, 1993: Is the magnitude of the deep outflow from the Atlantic Ocean actually governed by Southern Hemisphere winds? *The Global Carbon Cycle*, M. Heimann, Ed., NATO ASI Series, Vol. 15, Springer, 333–366.

Trenberth, K. E., and J. M. Caron, 2001: Estimates of meridional atmosphere and ocean heat transports. *J. Climate*, **14**, 3433–3443, https://doi.org/10.1175/1520-0442(2001)014<3433:EOMAAO>2.0.CO;2.

Veronis, G., 1973: Model of the world ocean circulation: I. Wind-driven, two layer. *J. Mar. Res.*, **31**, 228–288.

Wolfe, C. L., and P. Cessi, 2010: What sets the strength of the middepth stratification and overturning circulation in eddying ocean models? *J. Phys. Oceanogr.*, **40**, 1520–1538, https://doi.org/10.1175/2010JPO4393.1.

Young, W. R., 2012: An exact thickness-weighted average formulation of the Boussinesq equations. *J. Phys. Oceanogr.*, **42**, 692–707, https://doi.org/10.1175/JPO-D-11-0102.1.